Article

A Sustainable Forage-Grass-Power Fuel Cell Solution for Edge-Computing Wireless Sensing Processing in Agriculture 4.0 Applications

Johan J. Estrada-López [1], Javier Vázquez-Castillo [2], Andrea Castillo-Atoche [3], Edith Osorio-de-la-Rosa [4], Julio Heredia-Lozano [5] and Alejandro Castillo-Atoche [5,*]

1 Faculty of Mathematics, Autonomous University of Yucatan, Mérida 97000, Mexico; johan.estrada@correo.uady.mx
2 Informatics and Networking Department, Universidad Autónoma del Estado de Quintana Roo, Chetumal 77019, Mexico
3 Chemistry and Biochemistry Department, Tecnológico Nacional de México/Instituto Tecnológico de Mérida, Mérida 97118, Mexico
4 Informatics and Networking Department, CONACYT-Universidad Autónoma del Estado de Quintana Roo, Chetumal 77019, Mexico
5 Mechatronics Department, Autonomous University of Yucatan, Mérida 97000, Mexico
* Correspondence: acastill@correo.uady.mx

Abstract: Intelligent sensing systems based on the edge-computing paradigm are essential for the implementation of Internet of Things (IoT) and Agriculture 4.0 applications. The development of edge-computing wireless sensing systems is required to improve the sensor's accuracy in soil and data interpretation. Therefore, measuring and processing data at the edge, rather than sending it back to a data center or the cloud, is still an important issue in wireless sensor networks (WSNs). The challenge under this paradigm is to achieve a sustainable operation of the wireless sensing system powered with alternative renewable energy sources, such as plant microbial fuel cells (PMFCs). Consequently, the motivation of this study is to develop a sustainable forage-grass-power fuel cell solution to power an IoT Long-Range (LoRa) network for soil monitoring. The *stenotaphrum secundatum* grass plant is used as a microbial fuel cell proof of concept, implemented in a 0.015 m^3-chamber with carbon plates as electrodes. The BQ25570 integrated circuit is employed to harvest the energy in a 4 F supercapacitor, which achieves a maximum generation capacity of 1.8 mW. The low-cost pH SEN0169 and the SHT10 temperature and humidity sensors are deployed to analyze the soil parameters. Following the edge-computing paradigm, the inverse problem methodology fused with a system identification solution is conducted, correcting the sensor errors due to non-linear hysteresis responses. An energy power management strategy is also programmed in the MSP430FR5994 microcontroller unit, achieving average power consumption of 1.51 mW, ~19% less than the energy generated by the forage-grass-power fuel cell. Experimental results also demonstrate the energy sustainability capacity achieving a total of 18 consecutive transmissions with the LoRa network without the system's shutting down.

Keywords: Agriculture 4.0; edge computing; energy harvesting; IoT; plant microbial fuel cells; wireless sensor networks

1. Introduction

The growth of the Internet of Things (IoT) has had a significant impact on the development of novel wireless sensor networks (WSNs) and their applications in areas such as smart cities [1,2], structural health monitoring [3,4], precision agriculture [5,6], and smart homes [7,8]. More recently, the application of edge computing is being considered essential for the development of high-performance IoT and WSN platforms [9,10]. With the increasing amount of data that sensor nodes are expected to handle, the application of the edge-computing paradigm in end devices has emerged as a solution to simplify IoT

networking. Edge-computing responds to ever-increasing bandwidth demands and privacy concerns of IoT, to collect, analyze, and process data closer to end devices, and more efficiently than traditional cloud architectures [11]. However, this calls for edge devices with more computational power that can deliver the required advanced data processing and analytic methods in a flexible, efficient, and sustainable way [12].

Concerning this need for sustainable edge-based data acquisition and processing, different approaches have been studied already, such as energy-aware [13] and task scheduling [14] techniques. In particular, energy harvesting (EH) [15] looks as a promising approach to achieve edge-computing hardware powered by renewable energy sources, without the need of batteries. Recent studies focus on reducing the dependency on batteries in edge devices through the application of various techniques [16–18]. In [16], an analysis of EH technologies and their potential power densities for edge devices is provided. In [17], a mixed-integer linear programming technique is built to treat the problem of multitasking by considering minimum energy consumption and multitasking scheduling in software-defined sensor networks. Deep reinforcement learning (DRL)-based algorithms were proposed for dynamic computation offloading on mobile edge computing (MEC) with EH [18]. Previous results show that diverse edge devices can achieve a good balance between wireless transmission time and consumed energy, and demonstrate a significant improvement in performance when compared with baseline algorithms. However, previous works are limited to conventional EH technologies, such as photovoltaic, and there is still a need of analyzing the power generation capacity of novel renewable sources, and their suitability for the design of battery-less edge sensor nodes. Recent studies have demonstrated that Plant Microbial Fuel Cells (PMFCs) are an emerging and environmentally friendly technology that generates bioelectricity in the rhizosphere region of plants [19–22]. The bioelectricity generation has been improved by integrating Graphene Quantum Dots (GQD) into the soil at the root zone of plants. GQD materials promote power generation by the redox reaction from plant roots [19]. The effects of rhizodeposition and photosynthetic activity were also explored with a *C. indica*-based PMFC, achieving a power generation capacity of 2.72 mW [20]. A three-chamber modular structure is also tested for bioelectricity generation using a PMFC anodic chamber between two cathodes with an agar-based solid-state nutrient. Bentonite/flyash-based clay operates like the ion-exchange membrane, which is crucial to improve the performance of PMFCs [21]. Another approach for PMFC power generation is proposed in [22], investigating the effects of soil water content and temperature on the *Purple Guinea* forage grass. However, while these studies represent the state-of-the-art in PMFC bioelectricity generation, they do not address the integration of an energy harvester or wireless monitoring systems that can optimally extract the energy and transmit information to the cloud, in line with the IoT paradigm.

Therefore, the challenge tackled in this work is to develop a forage-grass-power fuel cell solution for powering edge-computing devices. In particular, the power generation capacity of the *stenotaphrum secundatum* grass-type PMFC is investigated and quantified in terms of the number of successfully transmitted packets of a Long Range (LoRa) network. For this purpose, a fuel cell based on a grass-type array of plants was designed, fabricated, and electrically characterized. The fuel cell is also used to energize the sensor node that performs soil analysis for agricultural applications.

The energy harvested by the PMFC is managed for data acquisition, LoRa transmission and data processing with the constrained optimization algorithm solution. The edge computing approach demonstrates the feasibility to perform inverse problem solutions with an energy sustainable behavior.

Figure 1 illustrates the conceptualization of the proposed forage-grass-power fuel cell proof of concept prototype for edge-computing wireless sensing processing. The contributions of this study can be summarized as follows:

- A 0.015 m^3-single chamber prototype of a grass-forage fuel cell with carbon plates electrodes is developed, with a demonstrated maximum power generation of 1.8 mW.

- A proven capacity of up to 18 consecutive LoRa transmissions with the edge sensing device powered with the forage-grass-power fuel cell approach.
- An inverse problem phenomenology fused with a system identification solution for an accurate sensing response of soil analysis on each sensor node.
- A low-power consumption of 1.51 mW@ 0.457 mA for the edge sensing system based on the MSP430FR5994 microcontroller unit (MCU), which implements the constrained regularization algorithm fused with the system identification.
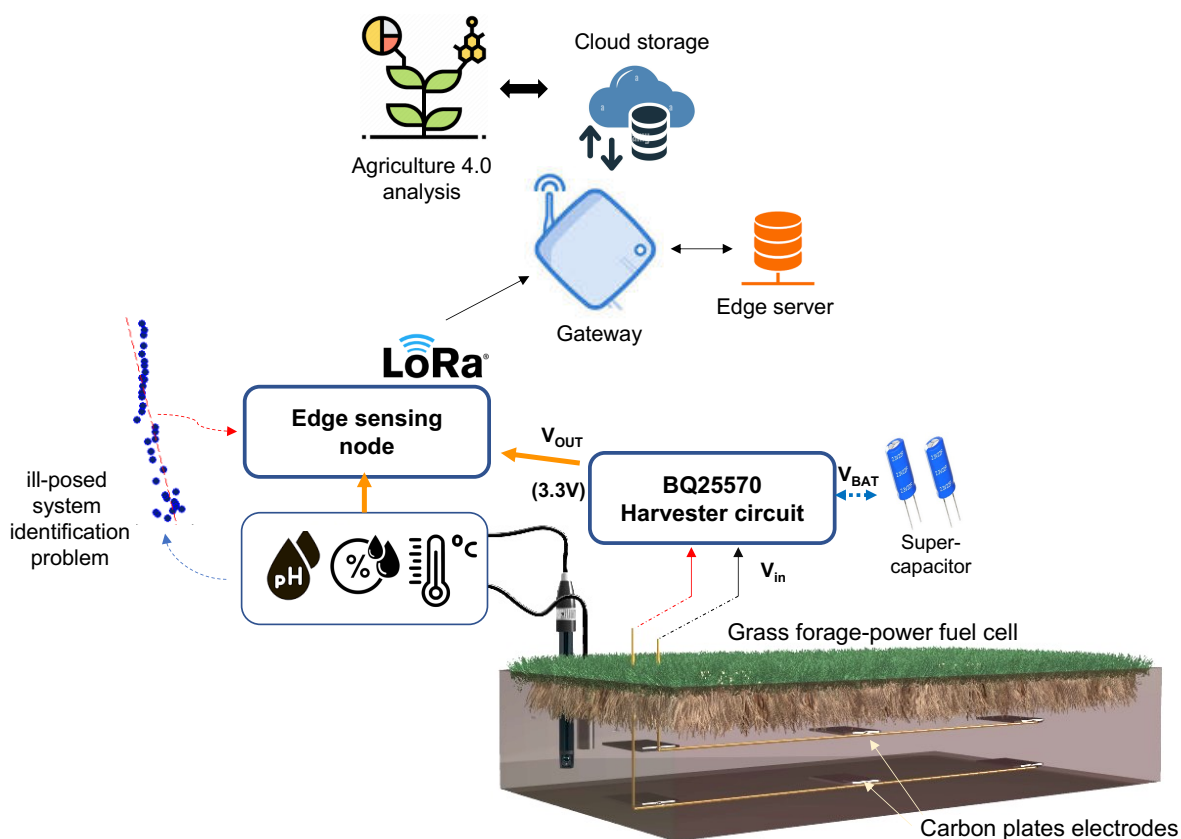

Figure 1. Conceptual idea of the proposed grass forage-power fuel cell for edge-computing wireless sensing.

The paper is organized as follows: Section 2 shows the fabrication of the forage-grass-power fuel cell solution to power the IoT sensing edge device. Section 3 describes the electronic embedded system and the inverse problem methodology processing. Section 4 presents the experimental results of the bio-electricity power generation capacity and the sustainability of the edge computing system. Finally, the discussion and concluding remarks are given in Sections 5 and 6, respectively.

2. Forage-Grass-Power Fuel Cell Structure Design and Characterization

Investigating the bio-electricity generation capacity of a grass-forage fuel cell is the motivation for the development of a proof of concept prototype design suitable for Agriculture 4.0 applications. The fuel cell fabrication, as well as the description of the energy harvesting circuit, are addressed in this section.

2.1. Stenotaphrum secundatum PMFC

The *Stenotaphrum secundatum* plant is a specie of the Gramineae family that is resistant to hot and humid weather conditions, and is particularly common in southeast Mexico. Traditionally, it is seen in landscapes and as an ornamental plant in gardens. The plant stems spread extensively over the ground surface, regularly producing roots, and the leaf

sheaths, i.e., 3 to 6 cm long, are mostly hairless. The dehydrogenase activity in soil with *stenotaphrum secundatum* is greater than in uncropped soil, which means more biomass production. Therefore, this PMFC represents an attractive option to harvest energy in outdoor environments, taking advantage of biomass metabolism as catalysts and the organic matter to generate bio-electrical energy [20].

2.2. Fuel Cell Fabrication

A low-cost single-chamber structure was constructed with acrylic material in a 15,000 cm^3-square pot container of dimensions $30 \times 50 \times 10$ cm, as depicted in Figure 2. The PMFC employs a mixture of 10 kg organic matter and 100 g industrial fertilizer.
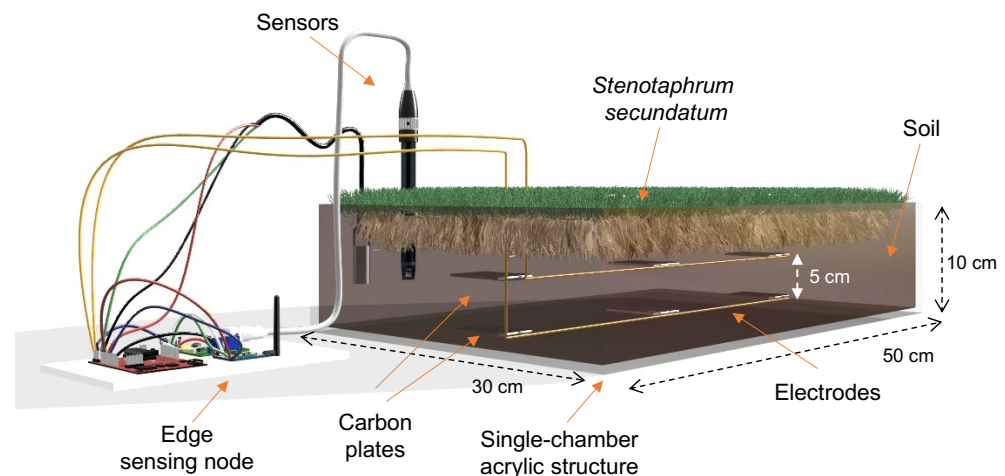

Figure 2. Prototype of the single-chamber grass forage-power fuel cell.

The PMFC electrodes' plates of dimension $4 \times 5 \times 0.2$ cm, are made of carbon. There were no holes at the bottom of the structure, keeping the soil immersed favoring conductivity. The distance between each pair of electrodes is 5 cm. According to [23], this distance gave a better performance in PMFCs.

Figure 3a describes the scalability of the PMFCs interconnected in parallel in the grass forage field. The deployment follows the Kirchhoff model of power sources as illustrated in Figure 3b. Each PMFC addresses the Randles equivalent circuit model [24] based on the physical understanding of the electrochemical processes occurring in the fuel cell. The Randles model contains a non-conductive interfacial capacitance working as an electric double layer and a pathway for electron transfer. This model represents the simplest electrode equivalent circuit, corresponding to a standard semi-circular arc when plotted on a single-arc Nyquist diagram. This phenomenon implies that a single-reaction process may be occurring in the PMFC [25].

The PMFC is electrochemically modeled as follows:

$$Z_{PMFC}(\omega) = R_{ir} + \frac{R_{ct} + W}{1 + j\omega C_{dl}(R_{ct} + W)} \tag{1}$$

where R_{ir} is the ionic resistance, R_{ct} is the charge transfer resistance, C_{dl} is the double layer capacitance, and W is the Warburg impedance.

The magnitude and the phase angle of the complex impedance are represented with a phasor diagram plotting the magnitude of the impedance vector as $|Z_{PMFC}|$ and the phase angle as θ. The impedance is expressed using its real and imaginary components as follows

$$|Z_{PMFC}(w)| = \sqrt{Zr^2 + Zj^2}. \tag{2}$$

The corresponding angle phase is

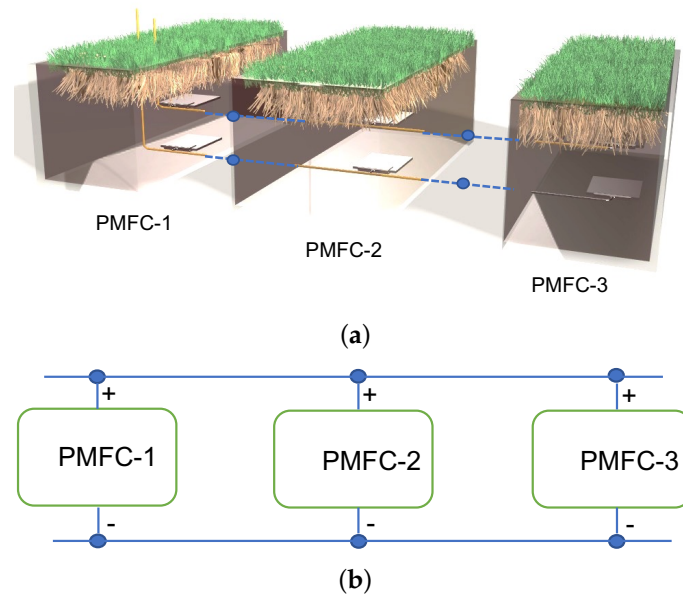$$\theta_{PMFC} = \tan^{-1}\left(\frac{Zj}{Zr}\right). \tag{3}$$

(a)

(b)

Figure 3. PMFC-based grass forage-power cell: (**a**) PMFC power array, and (**b**) equivalent PMFC schematic model.

2.3. Fuel Cell Characterization

The Metrohm Autolab electrochemical impedance spectroscopy equipment is used to characterize the PMFC array. The equipment tests in real-time the impedance diffusion of the forage-grass-power cell with a set of load resistances that analyze the extracted energy from the cell. Figure 4a compares the Randles diffusion model of Equation (1) and the measurements.

The real component of the impedance is represented in the *x*-axis of the Nyquist plot, and the imaginary component is plotted in the *y*-axis. Each point corresponds to the impedance at one frequency value. The following parameters $R_{ir} = 42\,\Omega$, $R_{ct} = 140\,\Omega$, $C_{dl} = 13.3\,\mu F$, and $W = 150\,\Omega$ were used in the analysis. Bode graphs are also shown with the dynamic behavior of the electrochemical impedance of the PMFC array in magnitude and phase in Figure 4b and Figure 4c, respectively. The Bode plots describe an accurate response of the PMFC array when compared with the calculated parameters of the Randles model.
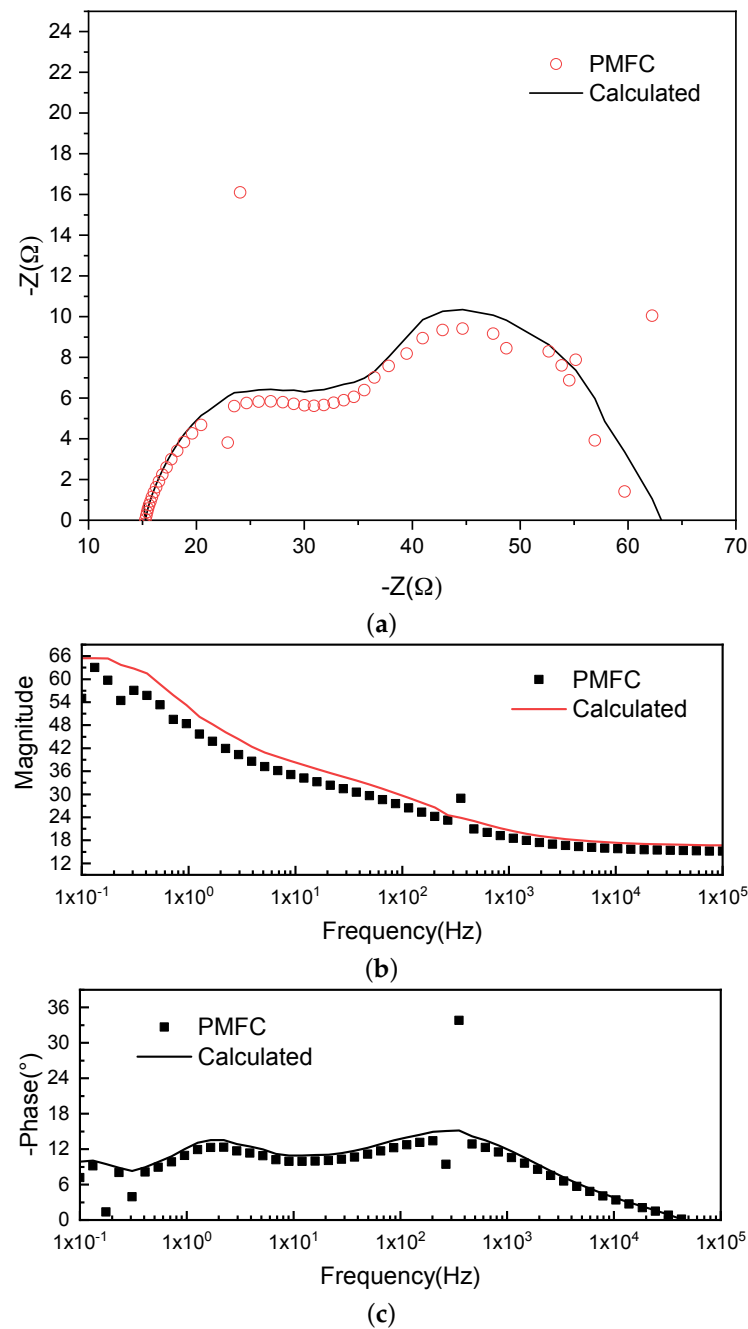
(a)

(b)

(c)

Figure 4. Comparative plots of the PMFC impedance analysis from the experimental and modeled data: (**a**) Nyquist plot of the PMFC array at maximum power point, (**b**) Bode impedance magnitude, and (**c**) impedance phase.

3. Self-Powered Edge Computing System and Inverse Problem Framework

A sustainable electronic edge computing system is described in this section as a viable solution for intelligent self-sensing Lora networks in Agriculture 4.0 applications. The power generated by the grass forage-power fuel cell is harvested and managed for the edge wireless system, which represents a reliable power fuel cell solution. Figure 5 illustrates the single-chamber forage-grass-power fuel cell prototype integrated with the edge-computing LoRa self-sensing system.
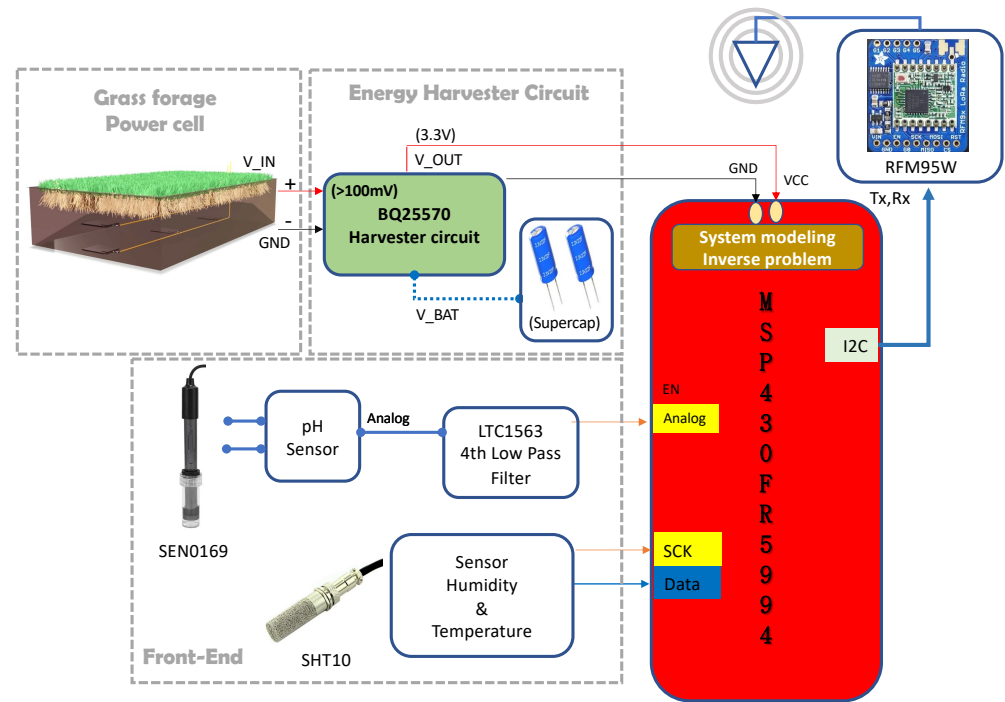
Figure 5. Self-powered edge computing system by the single-chamber forage-grass-power fuel cell.

3.1. Energy Harvester Circuit

The forage-grass-power fuel cell generates bioelectricity from the biodegradation of plant root exudates, rhizodeposits, and organic matter in the soil. The bacteria and microbes in the rhizosphere produce exudates that act as substrates and donate electrons to the anode via electron transfer [26]. This generated current and voltage vary depending on the absorbed energy in the carbon plates of the proposed PMFC. The BQ25570 is an integrated circuit EH solution that can be used to efficiently acquire and manage the bioenergy power generated from the PMFC.

The circuit shown in Figure 6 converts the bioenergy from the PMFC array with the DC/DC boost converter. The boost converter starts working with an input voltage V_IN down to 330 mV, and can continuously harvest energy from inputs as low as 100 mV.
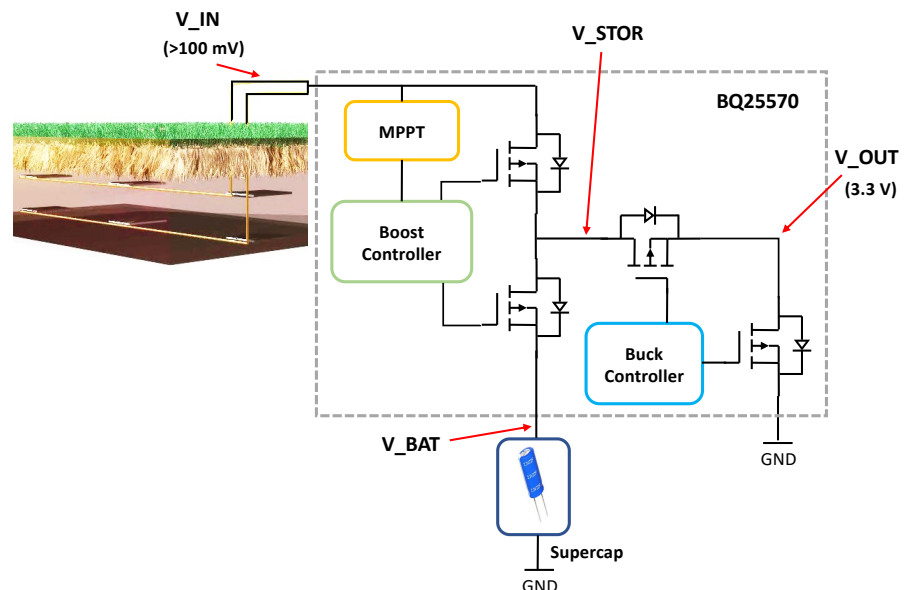

Figure 6. Energy harvesting circuit with the BQ25570.

The BQ25570 also implements a programmable maximum power point tracking (MPPT) algorithm to optimize the power transfer of the PMFCs. The sampled voltage for the MPPT is controlled via external resistor and capacitors to the circuit.

The boost circuit of the BQ25570 amplifies the input voltage from the grass forage-power cell to a predefined voltage level that charges a supercapacitor. The charging voltage is set to V_STOR equal to 4.2 V with external resistors. On the other hand, the buck converter circuit regulates the output voltage V_OUT to 3.3 V providing high efficiency across low- to high-output currents, i.e., $\leq$10 µA to $\sim$110 mA, respectively.

3.2. Front-End and Sensors

A low-cost pH sensor SEN0169 is employed in the sensing node with a typical power consumption of 3.0 mA. The LTC1563 is used to filter the pH signal, through an active Butterworth 4th-order low-pass filter with a 256 Hz cutoff frequency. This integrated circuit can be configured in shutdown mode, reducing its current consumption to 1 µA. The SEN0169 measures the pH response, which quantifies the nutrients and chemicals that are soluble in soil water, and, therefore, the available nutrients in plants. Remark that some nutrients are available under acid conditions while others are under alkaline conditions [27,28]. The temperature and humidity of the soil are measured with the SHT10 sensor. The SHT10 has a 12-bit digital output with a typical resolution of 0.05% RH (humidity) and 0.01 °C (temperature). It operates with a supply voltage range of 2.4–5.5 V, with a typical current consumption of 0.9 mA, and a guaranteed maximum of 1.5 µA when it is put to sleep. Temperature, humidity, and pH in the soil play a key role in crop quality estimation. However, uncertainties in the measurements due to the variability of minerals and dry plant tissue make it necessary to re-calibrate the sensors. Intelligent system management is conducted to improve the measurement reliability during system operation following the inverse problem phenomenology with the parametric system identification to build a mathematical model from the measured data.

3.3. Wireless Communication Module

The RFM95W LoRa transceiver is used for local communication from the edge sensing node to the gateway. The LoRaWAN-Class A protocol operates in the 915 MHz unlicensed band, being able to transmit up to a distance of 3 km in line of sight or up to 20 km with directional antennas. The LoRaWAN wireless technology offers a balance in power consumption and range coverage, even though other popular stacks, such as narrowband IoT (NB-IoT) and long-term evolution (LTE), are good candidates. However, NB-IoT operates on the existing global system for mobile (GSM), and the LTE network use licensed frequency bands. Both options have larger power consumptions [29].

3.4. Low-Power Edge Computing Controller

The selected MSP430FR5994 is a 16-bit ultra-low-power MCU designed for applications with low energy budgets in mind. For example, with a 3.3 V suppy, its sleep (LPM3) and shut-down (LPM3.5) modes consume a maximum current of 0.4 µA and 0.25 µA, respectively, while the active mode has a typical current consumption of 400 µA. The maximum time required by the MCU to wake up from sleep mode is 6 µs. In addition, its hardware includes mixed signal capability, a non-volatile Ferroelectric Random Access Memory (FRAM) of 256 KB, and a Low-Energy Accelerator (LEA) that delivers fast and efficient vector math acceleration required in sensing and edge-computing applications.

3.4.1. System Modeling

The ill-posed nature of an inverse problem is alleviated by employing the parametrization idea as a descriptive regularization method. This ill-posed essence is due to sensing data acquisition errors, the diffuse nature of the soil conditions, and numerical modeling er-

rors. The observation model is formulated assuming the inverse problem phenomenology, as follows:

$$\mathbf{u} = \mathbf{S}(\boldsymbol{\rho}) + \boldsymbol{\epsilon}, \tag{4}$$

where $\mathbf{S}$ is the unknown inertia-less transform matrix of an input vector $\boldsymbol{\rho}$, and $\boldsymbol{\epsilon}$ is the random noise in measurements $\mathbf{u}$.

To solve the inverse problem in an intelligent system management approach, a parametric system identification based on the least-squares (LS) criterion is defined:

$$J(\boldsymbol{\rho}) = \min_{\boldsymbol{\rho}}\{||\mathbf{u} - \mathbf{S}(\boldsymbol{\rho}, \boldsymbol{\phi})||^2\} \tag{5}$$

where $|| \cdot ||$ is the Euclidean norm and $\mathbf{s}(\boldsymbol{\rho}, \boldsymbol{\phi})$ is considered to be a known function of variable $\boldsymbol{\rho}$ dependent on the vector of unknown parameters $\boldsymbol{\phi}$.

The strategy consists in comparing all the possible solutions that fit the input-output data of the system $\{u_k, \rho_k; k = 1, ..., K\}$ for the hypothesis model, and then make a choice in such a way that the approximation error of $\mathbf{u}$ and the identified model $\mathbf{S}(\boldsymbol{\rho}, \boldsymbol{\phi})$ is the smallest. Here, the particular known system model $\mathbf{S}(\boldsymbol{\rho}, \boldsymbol{\phi}) = a\ln(\boldsymbol{\rho}) + b$, where $\boldsymbol{\phi} = (a, b)^{\mathrm{T}}$, is proposed. To handle the ill-posedness, partial derivatives of J are implemented with respect to $\{\phi_1 = a, \phi_2 = b\}$ and set these to zero, as presented in the next equation

$$\frac{\partial J}{\partial \phi_i} = (-2)\sum_{k=1}^{K}[u_k - s(\rho_k; a, b)]\frac{\partial s(\rho_k; \phi)}{\partial \phi_i} = 0; i = 1, 2; \phi_1 = a, \phi_2 = b. \tag{6}$$

The parameters $\hat{a}$ and $\hat{b}$ are estimated applying the linear regression problem to the partial derivatives as follows:

$$\hat{a} = \frac{K\sum \rho_k U_k - \sum \rho_k \sum U_k}{K\sum \rho_k^2 - (\sum \rho_k)^2}, \tag{7}$$

$$\hat{b} = \frac{1}{K}(U_k - \hat{A}\sum \rho_k). \tag{8}$$

where variables $(u = U, v = V, a = A, b = B)$, model $\mathbf{S}(\boldsymbol{\rho}, \boldsymbol{\phi}) \rightarrow \hat{a} = \hat{A}, \hat{b} = \hat{B}$.

A software library is developed for the selected microcontroller unit, containing the estimated parameters and mathematical operations of the inverse problem fused system identification solution presented above for accurate soil measurements.

3.4.2. Power Management Strategy

In this subsection, the power management strategy is modeled as a finite state machine to reduce the power consumption of the edge-computing sensing node. The sensing node operation is the following: at every sample, the measurements of the SHT10 and the SEN0169 sensors are acquired, and processed with our proposed system identification (SI) model. Data are next transmitted to the cloud with the LoRaWAN protocol. Once data are transmitted, the MCU returns to the sleep state for 15 min. This power management strategy, implemented in the MCU, is modeled as a finite state machine (FSM) to reduce the power consumption of the sensing node operation, and, in consequence, improve the energy management of the sensing system. Figure 7 illustrates the state transition graph (STG) of the proposed power management strategy approach.

The proposed strategy consists on turning on and off some system's components in a specific sequence, while putting all the other circuitry into Sleep Mode [30]. This methodology saves energy and extends the sensor node's battery life. The energy-optimized operating states of the sensor node are called low-power modes; i.e., LPM0 and LPM4, where the MCU is configured in standby and sleep mode, respectively. The active mode sequentially acquires, process, and transmit the data. The standby mode occurs between the sleep and the active state, as illustrated in Figure 7.
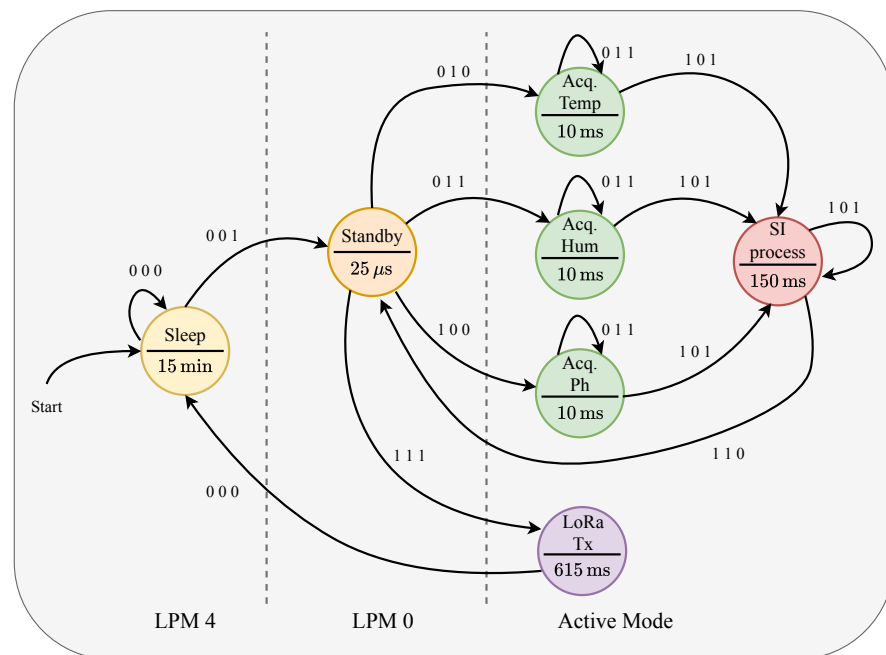
Figure 7. State transition graph of the power management strategy.

A state transition table (STT) is used to analyze the affections of input conditions on the system's state or output changes. STT, in Table 1, helps to analyze the power management behavior for different input conditions. This description is implemented in C++ language for low-power consumption of the MSP430FR5994 MCU and compiled with the Texas Instruments Code Composer Studio (CCS) design suite.

Table 1. STT analysis.

	Inputs							
States	**000**	**001**	**010**	**011**	**100**	**101**	**110**	**111**
Sleep	–	Stdby	–	–	–	–	–	–
Stdby	–	–	Acq. Temp	Acq. Hum	Acq. pH	–	–	LoRaTx
Acq. Temp	–	–	–	–	–	SI process	–	–
Acq. Hum	–	–	–	–	–	SI process	–	–
Acq. pH	–	–	–	–	–	SI process	–	–
SI process	–	–	–	–	–	–	Stdby	–
LoRa Tx	Sleep	–	–	–	–	–	–	–

– => unchanged state.

Algorithm 1 shows the pseudo-code implementation of the power management strategy programmed in the MSP430FR5994 MCU. The STG and the STT models provide a mathematical representation with the aim of energy-saving, while still allowing a more frequent monitoring of the soil when compared with previous works that propose longer sleep periods of 30 to 60 min [31]. The measured data show that a minimum period of 10 min results in a good trade-off for our specific study for Agriculture 4.0 applications.

Algorithm 1 FSM pseudo-code of the power management

Initialization: Sleep state

```
typedef const struct State State_t;
#define    Sleep    &FSM[0]
#define    Stdby    &FSM[1]
#define    AcqTemp    &FSM[2]
#define    AcqTemp    &FSM[3]
#define    AcqpH    &FSM[4]
#define    SIprocess    &FSM[5]
#define    LoRaTx    &FSM[6]
State_t    FSM[7] =
   dir1,t1,{Sleep, Stdby, Sleep, Sleep, Sleep, Sleep, Sleep,Sleep},
   dir2,t2,{Stdby, Stdby, AcqTemp, AcqHum, AcqpH, Stdby, Stdby,LoRaTx},
   dir3,t3,{AcqTemp, AcqTemp, AcqTemp, AcqTemp, AcqTemp, SIprocess, AcqTemp,
AcqTemp},
   dir4,t3,{AcqHum, AcqHum, AcqHum, AcqHum, AcqHum, SIprocess, AcqHum, Ac-
qHum},
   dir5,t3,{AcqpH, AcqpH, AcqpH, AcqpH, AcqpH, SIprocess, AcqpH, AcqpH},
   dir6,t1,{SIprocess,  SIprocess,  SIprocess,  SIprocess,  SIprocess,  SIprocess,
Stdby,SIprocess}
   dir6,t4,{Sleep, LoRaTx, LoRaTx, LoRaTx, LoRaTx, LoRaTx, LoRaTx,LoRaTx};
void main(void) {
   uint32_t cs;    uint32_t input;
   initialize_ports_timer();
   cs = Sleep;
```

while (1) **do**

```
   //1) Wakeup from sleep state
   LPM0(); Delay(FSM[cs].Time); cs = Stdby;
   // 2) Data acquisition
   AM(); DataAcq(); Delay(FSM[cs].Time); cs = AcqTemp | AcqHum | AcqpH;
   // 3) System Identification processing
   AM(); SIprocess(); Delay(FSM[cs].Time); cs = SIprocess;
   // 4) Standby state
   LPM0(); LoRaTx(); Delay(FSM[cs].Time); cs = LoRaTx;
   // 5) LoRa transmission
   AM(); Delay(FSM[cs].Time);cs = Sleep;
   // 6) Sleep state
   LPM4(); Delay(FSM[cs].Time);cs = Stdby;
```

end while

```
   }
```

---

4. Experimental Results

The power generation capacity of the grass forage-power fuel cell is presented in this section, demonstrating the sustainable operation of the edge-computing wireless sensing network. The energy harvested from the array of P-MFCs and the power management strategy provides 19% more energy than the energy consumed by sensors, the inverse problem processing, and the LoRa transceiver. The self-powered operation is also presented in terms of the number of packets transmitted in an IoT-LoRa network. Figure 8 illustrates the prototype of the grass forage-power fuel cell powering a single-edge wireless sensing device.
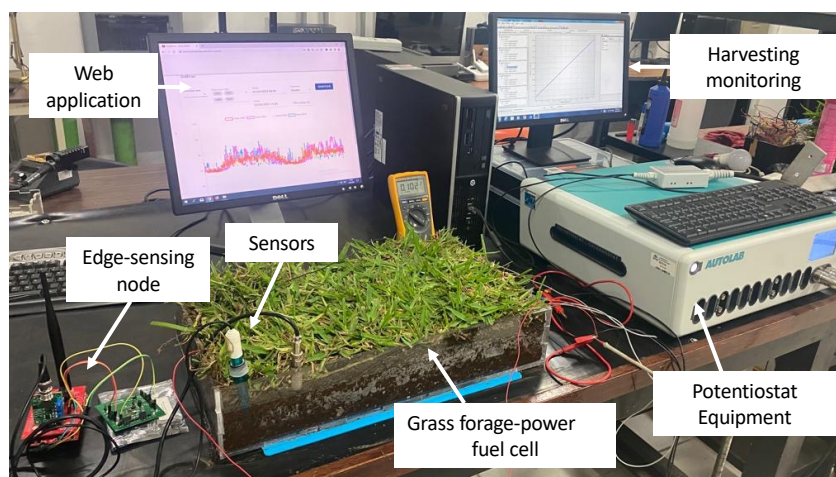
Figure 8. Prototype of the grass forage-power cell system.

4.1. Grass Forage-Power Generation Results

The forage-grass-power cell was evaluated by analyzing the polarization curves under laboratory conditions operating the PMFC array at the maximum power point. In the experiment, the power cell was evaluated with the Metrohm Autolab Potentiostat. Figure 9 shows the current and power density curves in terms of the voltage. A maximum power and current generation of up to ~1.8 mW and ~10 mA were achieved. In the experimental analysis, the P-MFC array impedance was measured with the potentiostat equipment finding an accurate response according to the Randles model of Equation (1).
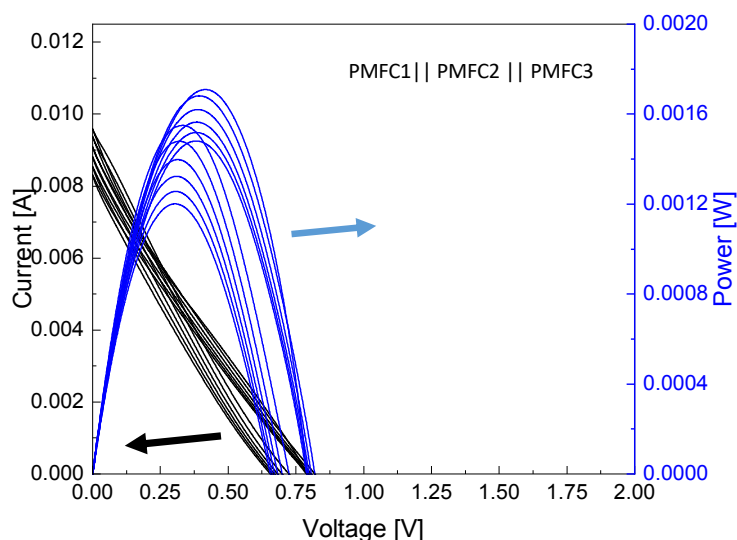

Figure 9. Forage-grass-power fuel cell I-V analysis.

The power generation capacity is tested with the cold-start operation analysis. A 25 °C room temperature and the light adjusted to 2000 lux, were set for the test. Figure 10 shows the supercapacitor charging time when the storage element is completely discharged. The forage-grass-power fuel cell charges the 4 F supercapacitor at 4.2 V in only 15 h.

From the analysis of Figure 10, one can notice that the harvester circuit achieves 1.8 V in 11.6 h, and the main booster on the bq25570 extracts the energy more efficient to charge up the supercapacitor in only 3.4 h.
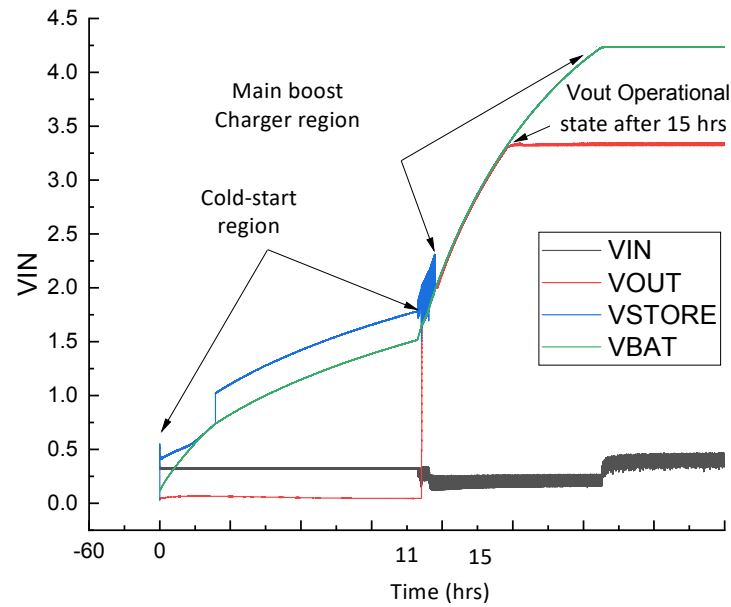
Figure 10. Cold start forage-grass-power cell analysis.

4.2. Edge Signal Processing Response

The parametric system identification (SI) technique was used to develop a mathematical system modeling approach, to increase process reliability, and reduce the hysteresis effect in the SEN0169 pH sensor response. From all possible strain gradients related to the pH dispersion, the proposed SI model $\mathbf{S}(\boldsymbol{\rho}, \boldsymbol{\phi}) = a\ln(\boldsymbol{\rho}) + b$ identifies the best statistical curve as a solution to an ill-posed problem. This is illustrated in Figure 11. The coefficients a = 4.038, and b = 0.306 were calculated following Equations (7) and (8).
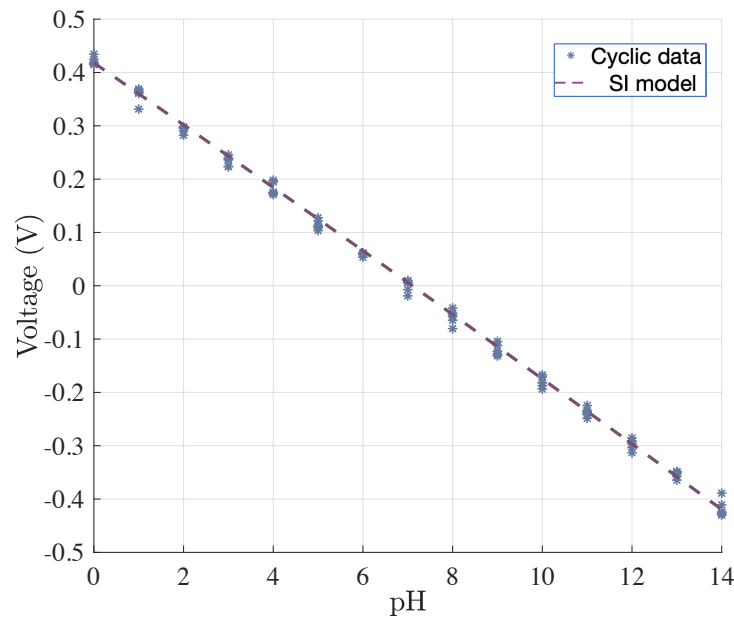

Figure 11. SI model analysis.

To convert the digital readout data SO_T coming from the SHT10 sensor, the following equation was implemented in the MCU to calibrate the temperature measurement:

$$T_{\circ C} = d_1 + d_2 * SO_T + d_{Ti10}, \tag{9}$$

where $d_1 = 39.7\,°C$, $d_2 = 0.04$ and $d_{Ti10} = 0.001\,°C$, which represents the calibration offset of the sensor.

The humidity sensor's non-linearity can be compensated using the following equation:

$$\%\text{RH} = c_1 + c_2 \cdot SO_{RH} + c_3 \cdot SO_{RH}^2 \tag{10}$$

where $c_1 = -2.0468$, $c_2 = 0.0367$, $c_3 = -1.5955 \times 10^{-6}$ and SO_{RH} is the measured value of humidity. Temperature compensation is also required when measuring the humidity. This can be performed using the following correction equation:

$$\%\text{RH}_C = (T_{°C} - 25) \cdot (t_1 + t_2 \cdot SO_{RH}) + \%\text{RH} \tag{11}$$

where $t_1 = 0.01$ and $t_2 = 0.00008$, and $\%\text{RH}_C$ is the relative humidity measurement with temperature compensation.

4.3. Power Consumption of the Sensing Node

The Code Composer Studio platform includes the EnergyTrace++ tool, which was used for the real time measurement and analysis of the LoRa edge sensing node's power consumption. Table 2 presents the measurement results of the sensing node operating in all processing states.

Table 2. Power consumption analysis of the edge-computing wireless sensing node.

Single-Edge Sensing Node States	Power Consumption
Sleep state (MCU) and peripherals turn-off	0.32 mW @ 96.9 μA
Sensing on	14 mW @ 4.2 mA
MCU SI processing	6.12 mW @ 1.85 mA
LoRa transmission	228 mW @ 69 mA
Complete Sensor Node System	**Average Power Consumption**
	1.51 mW @ 457.5 μA

Observe that the inverse problem system identification algorithm has a measured power consumption of 6.12 mW, which is less than the sensing state consumption (14 mW) state, due to the application of the finite state machine algorithm for the power management strategy. The LoRa transceiver is active for data transmission for 617 ms, with a consumption of 228 mW. Even with this peak power demanded by the transmitter during a short time, the average consumption of the edge-computing sensing node is only 1.51 mW. This is the result of configuring the MCU in ultra-low-power mode during the sleep state of 15 min, with all the peripherals disconnected and turned off.

The power generation result of the grass forage-power cell is 1.8 mW, which means $\sim 1.19\times$ the required power of the LoRa wireless node. Therefore, it can be concluded that the grass forage-power cell can generate the energy for an autonomous performance, achieving a perpetual battery-less operation.

5. Sustainability Discussion and Power Capacity Interpretation

In terms of power generation capacity, the edge-computing wireless system is able to perform 18 consecutive LoRa transmissions once the 4F supercapacitor is fully charged. However, although the power generation capacity seems to be stable, the water content in the soil, humidity, temperature, and other conditions could cause the power generation to decrease over several days. A dynamic power management strategy is recommended for future study, to regulate the sensor node duty cycle, maximizing the number of LoRa transmissions and guaranteeing sustainable operation.

Table 3 presents an analysis of the power capacity of the forage-grass-power fuel cell for IoT systems, in comparison to other similar works. The studies in [19–22] developed PMFC-based fuel cells. Xu et al. [19] integrated graphene quantum dots to enhance the

power capacity of the fuel cell in the soil at the root zone of the plant. Although their power generation of 4.84 mW is higher than our system, they employed a large array of PMFCs, i.e., a green wall, as a power source. An attractive three-chamber modular structure for bioelectricity generation using a PMFC anodic chamber between two cathodes with an agar-based solid-state nutrient was proposed in [21]. The advantage of this power cell is the Bentonite/flyash-based clay that operates like the ion-exchange membrane. However, they did not incorporate the harvester circuit. The studies in [20,22] presented PMFC-based power cell implementations with carbon cloth electrodes. However, a wireless embedded processing approach is not included.

Table 3. PMFC comparative analysis.

Reference	Plant Type	Number of PMFCs	Power Generation	Electrodes	Harvester Circuit	Wireless Communication
[19]	*Zephyranthes Grandflora*	Array	4.84 mW	Graphene Quantum Dots	–	WiFi
[20]	*C. indica*	3	2.72 mW	Carbon Cloth	–	–
[21]	*Epipremnum aureum*	–	1.48 mW	Carbon Cloth	–	–
[22]	*Purple guinea*	–	1.53 mW	Carbon Cloth	–	–
This Work	*Stenotaphrum secundatum*	3	1.8 mW	Carbon Plates	Bq25570	LoRa

6. Conclusions

A sustainable forage-grass-power fuel cell solution to power an IoT LoRa network for soil analysis was proposed. In this regard, a 0.015 m^3-single chamber prototype using the *stenotaphrum secundatum* plant-type with carbon plate electrodes was designed and electrically characterized to power the edge computing devices of the sensing nodes. The edge-sensing system based on the MSP430FR5994 MCU has a low power consumption level of 1.51 mW@ 0.457 mA, and the BQ25570 harvester circuit achieves a maximum generation capacity of 1.8 mW. In terms of sustainability, the generated energy by the forage-grass-power cell is ∼19% more than the single-edge wireless sensing node consumption. In terms of IoT systems, this energy is capable to implement up to 18 consecutive transmissions with a LoRa network without the system's shutting down. Likewise, an inverse problem methodology with a system identification was proposed and implemented following the edge computing paradigm. This methodology aims to correct the sensor's errors due to non-linear system parameters to provide accurate responses. In order to save the system's consumption, an energy power management strategy was programmed in the low-power Texas Instruments MSP430FR5994 microcontroller unit, which was powered by the PMFC-based fuel cell, demonstrating the feasibility to develop inverse problem solutions in the edge sensing node device. Experimental results show the energy sustainability capacity of the forage-grass-based power fuel cell prototype and the power management strategy, allowing to perform inverse problem solutions to minimize sensing errors under the edge-computing paradigm in wireless sensing networks for Agriculture 4.0 applications.

Author Contributions: Methodology, J.H.-L.; Formal analysis, E.O.-d.-l.-R.; Data curation, J.V.-C.; Writing—original draft, J.J.E.-L. and A.C.-A. (Alejandro Castillo-Atoche); Writing—review & editing, A.C.-A. (Andrea Castillo-Atoche). All authors have read and agreed to the published version of the manuscript.

Data Availability Statement: Data sharing not applicable.

Abbreviations

The following abbreviations are used in this manuscript:

CCS	Code Composer Studio
DRL	Deep Reinforcement Learning
DSP	Digital Signal Processing
EH	Energy Harvesting
FRAM	Ferroelectric Random Access Memory
FSM	Finite State Machine
GQD	Graphene Quantum Dots
GSM	Global System for Mobile
IoT	Internet of Things
LEA	Low-Energy Accelerator
LTE	Long Term Evolution
MCU	Microcontroller Unit
MEC	Mobile Edge Computing
MPPT	Maximum Power Point Tracking
NB-IoT	Narrow Band IoT
PMFC	Plant Microbial Fuel Cell
STG	State Transition Graph
STT	State Transition Table
WSN	Wireless Sensor Networks

References

1. Sharma, A.; Singh, P.K.; Kumar, Y. An integrated fire detection system using IoT and image processing technique for smart cities. *Sustain. Cities Soc.* **2020**, *61*, 102332. [CrossRef]
2. Ayala-Ruiz, D.; Castillo-Atoche, A.; Ruiz-Ibarra, E.; Osorio de la Rosa, E.; Vázquez-Castillo, J. A self-powered PMFC-based wireless sensor node for smart city applications. *Wirel. Commun. Mob. Comput.* **2019**, *2019*, 8986302. [CrossRef]
3. Muttillo, M.; Stornelli, V.; Alaggio, R.; Paolucci, R.; Di Battista, L.; de Rubeis, T.; Ferri, G. Structural health monitoring: An IoT sensor system for structural damage indicator evaluation. *Sensors* **2020**, *20*, 4908. [CrossRef]
4. Chang, H.F.; Shokrolah Shirazi, M. Integration with 3D visualization and IoT-based sensors for real-time structural health monitoring. *Sensors* **2021**, *21*, 6988. [CrossRef]
5. Kim, S.; Lee, M.; Shin, C. IoT-based strawberry disease prediction system for smart farming. *Sensors* **2018**, *18*, 4051. [CrossRef] [PubMed]
6. Akhtar, M.N.; Shaikh, A.J.; Khan, A.; Awais, H.; Bakar, E.A.; Othman, A.R. Smart sensing with edge computing in precision agriculture for soil assessment and heavy metal monitoring: A review. *Agriculture* **2021**, *11*, 475. [CrossRef]
7. Ghayvat, H.; Mukhopadhyay, S.; Gui, X.; Suryadevara, N. WSN- and IoT-based smart homes and their extension to smart buildings. *Sensors* **2015**, *15*, 10350–10379. [CrossRef]
8. Liu, H.; Li, S.; Sun, W. Resource allocation for edge computing without using cloud center in smart home environment: A pricing approach. *Sensors* **2020**, *20*, 6545. [CrossRef] [PubMed]
9. Minh, Q.N.; Nguyen, V.H.; Quy, V.K.; Ngoc, L.A.; Chehri, A.; Jeon, G. Edge Computing for IoT-Enabled Smart Grid: The Future of Energy. *Energies* **2022**, *15*, 6140. [CrossRef]
10. Cruz, M.; Mafra, S.; Teixeira, E.; Figueiredo, F. Smart Strawberry Farming Using Edge Computing and IoT. *Sensors* **2022**, *22*, 5866. [CrossRef]
11. Saeed, A.; Khattak, M.A.K.; Rashid, S. Role of big data analytics and edge computing in modern IoT applications: A systematic literature review. In Proceedings of the 2022 2nd International Conference on Digital Futures and Transformative Technologies (ICoDT2), Rawalpindi, Pakistan, 24–26 May 2022; pp. 1–5. [CrossRef]
12. Xu, J.; Palanisamy, B.; Wang, Q.; Ludwig, H.; Gopisetty, S. Amnis: Optimized stream processing for edge computing. *J. Parallel Distrib. Comput.* **2022**, *160*, 49–64. [CrossRef]
13. Jiang, C.; Fan, T.; Gao, H.; Shi, W.; Liu, L.; Cérin, C.; Wan, J. Energy aware edge computing: A survey. *Comput. Commun.* **2020**, *151*, 556–580. [CrossRef]
14. Zhang, J.; Zhou, X.; Ge, T.; Wang, X.; Hwang, T. Joint Task Scheduling and Containerizing for Efficient Edge Computing. *IEEE Trans. Parallel Distrib. Syst.* **2021**, *32*, 2086–2100. [CrossRef]
15. Zeng, D.; Pan, S.; Chen, Z.; Gu, L. An MDP-Based Wireless Energy Harvesting Decision Strategy for Mobile Device in Edge Computing. *IEEE Netw.* **2019**, *33*, 109–115. [CrossRef]
16. Sharma, A.; Sharma, P. Energy Harvesting Technology for IoT Edge Applications. In *Smart Manufacturing*; Kheng, T.Y., Ed.; IntechOpen: Rijeka, Croatia, 2021; Chapter 6. [CrossRef]

17. Zeng, D.; Li, P.; Guo, S.; Miyazaki, T.; Hu, J.; Xiang, Y. Energy Minimization in Multi-Task Software-Defined Sensor Networks. *IEEE Trans. Comput.* **2015**, *64*, 3128–3139. [CrossRef]

18. Zhang, J.; Du, J.; Shen, Y.; Wang, J. Dynamic computation offloading with energy harvesting devices: A hybrid-decision-based deep reinforcement learning approach. *IEEE Internet Things J.* **2020**, *7*, 9303–9317. [CrossRef]

19. Xu, Y.; Lu, Y.; Zhu, X. Toward Plant Energy Harvesting for 5G Signal Amplification. *ACS Sustain. Chem. Eng.* **2021**, *9*, 1099–1104. [CrossRef]

20. Nitisoravut, R.; Regmi, R. Plant microbial fuel cells: A promising biosystems engineering. *Renew. Sustain. Energy Rev.* **2017**, *76*, 81–89. [CrossRef]

21. Sarma, P.; Malakar, B.; Mohanty, K. Self-sustaining bioelectricity generation in plant-based microbial fuel cells (PMFCs) with microalgae-assisted oxygen-reducing biocathode. *Biomass Conv. Bioref.* **2023**. [CrossRef]

22. Nguyen, V.; Nitisoravut, R. Bioelectricity Generation in Plant Microbial Fuel Cell Using Forage Grass under Variations of Circadian Rhythm, Ambient Temperature, and Soil Water Contents. In Proceedings of the 2019 IEEE Asia Power and Energy Engineering Conference (APEEC), Chengdu, China, 29–31 March 2019; pp. 240–244. [CrossRef]

23. Takanezawa, K.; Nishio, K.; Kato, S.; Hashimoto, K.; Watanabe, K. Factors Affecting Electric Output from Rice-Paddy Microbial Fuel Cells. *Biosci. Biotechnol. Biochem.* **2010**, *74*, 1271–1273. [CrossRef]

24. Harrington, D.A.; van den Driessche, P. Mechanism and equivalent circuits in electrochemical impedance spectroscopy. *Electrochim. Acta* **2011**, *56*, 8005–8013. [CrossRef]

25. Wang, H.; Long, X.; Sun, Y.; Wang, D.; Wang, Z.; Meng, H.; Jiang, C.; Dong, W.; Lu, N. Electrochemical impedance spectroscopy applied to microbial fuel cells: A review. *Front. Microbiol.* **2022**, *13*, 973501. [CrossRef]

26. Chiranjeevi, P.; Yeruva, D.K.; Kumar, A.K.; Mohan, S.V.; Varjani, S. Chapter 3.8—Plant-Microbial Fuel Cell Technology. In *Microbial Electrochemical Technology*; Mohan, S.V., Varjani, S., Pandey, A., Eds.; Biomass, Biofuels and Biochemicals; Elsevier: Amsterdam, The Netherlands, 2019; pp. 549–564. [CrossRef]

27. Merl, T.; Rasmussen, M.R.; Koch, L.R.; Søndergaard, J.V.; Bust, F.F.; Koren, K. Measuring soil pH at in situ like conditions using optical pH sensors (pH-optodes). *Soil Biol. Biochem.* **2022**, *175*, 108862. [CrossRef]

28. Devkota, M.; Singh, Y.; Yigezu, Y.A.; Bashour, I.; Mussadek, R.; Mrabet, R. Chapter Five—Conservation Agriculture in the drylands of the Middle East and North Africa (MENA) region: Past trend, current opportunities, challenges and future outlook. *Adv. Agron.* **2022**, *172*, 253–305. [CrossRef]

29. Mekki, K.; Bajic, E.; Chaxel, F.; Meyer, F. A comparative study of LPWAN technologies for large-scale IoT deployment. *ICT Express* **2019**, *5*, 1–7. [CrossRef]

30. Ruan, T.; Chew, Z.J.; Zhu, M. Energy-Aware Approaches for Energy Harvesting Powered Wireless Sensor Nodes. *IEEE Sens. J.* **2017**, *17*, 2165–2173. [CrossRef]

31. Sánchez Fernández, L.P. Environmental noise indicators and acoustic indexes based on fuzzy modelling for urban spaces. *Ecol. Indic.* **2021**, *126*, 107631. [CrossRef]